Comparison of Freeboard Retrieval and Ice Thickness Calculation From ALS, ASIRAS, and CryoSat-2 in the Norwegian Arctic to Field Measurements Made During the N-ICE2015 Expedition

King, Jennifer; Skourup, Henriette; Hvidegaard, Sine M.; Rösel, Anja; Gerland, Sebastian; Spreen, Gunnar; Polashenski, Chris; Helm, Veit; Liston, Glen E.

Published in:
Journal of Geophysical Research: Oceans

Link to article, DOI:
10.1002/2017JC013233

Publication date:
2018

Document Version
Publisher's PDF, also known as Version of record

AGU PUBLICATIONS

JGR

Journal of Geophysical Research: Oceans

RESEARCH ARTICLE

10.1002/2017JC013233

Special Section:
Atmosphere-ice-ocean-ecosystem Processes in a Thinner Arctic Sea Ice Regime: The Norwegian Young Sea ICE Cruise 2015 (N-ICE2015)

Comparison of Freeboard Retrieval and Ice Thickness Calculation From ALS, ASIRAS, and CryoSat-2 in the Norwegian Arctic to Field Measurements Made During the N-ICE2015 Expedition

Jennifer King[1], Henriette Skourup[2], Sine M. Hvidegaard[2], Anja Rösel[1], Sebastian Gerland[1], Gunnar Spreen[3], Chris Polashenski[4], Veit Helm[5], and Glen E. Liston[6]

[1]Norwegian Polar Institute, Fram Centre, Tromsø, Norway, [2]DTU Space, Technical University of Denmark, National Space Institute, Lyngby, Denmark, [3]University of Bremen, Institute of Environmental Physics, Bremen, Germany, [4]U.S. Army Cold Regions and Engineering Laboratory, Alaska, Fort Wainwright, Alaska, USA, [5]Alfred Wegener Institute, Bremerhaven, Germany, [6]Cooperative Institute for Research in the Atmosphere, Colorado State University, Fort Collins, Colorado, USA

Abstract We present freeboard measurements from airborne laser scanner (ALS), the Airborne Synthetic Aperture and Interferometric Radar Altimeter System (ASIRAS), and CryoSat-2 SIRAL radar altimeter; ice thickness measurements from both helicopter-borne and ground-based electromagnetic-sounding; and point measurements of ice properties. This case study was carried out in April 2015 during the N-ICE2015 expedition in the area of the Arctic Ocean north of Svalbard. The region is represented by deep snow up to 1.12 m and a widespread presence of negative freeboards. The main scattering surfaces from both CryoSat-2 and ASIRAS are shown to be closer to the snow freeboard obtained by ALS than to the ice freeboard measured in situ. This case study documents the complexity of freeboard retrievals from radar altimetry. We show that even under cold (below −15°C) conditions the radar freeboard can be close to the snow freeboard on a regional scale of tens of kilometers. We derived a modal sea-ice thickness for the study region from CryoSat-2 of 3.9 m compared to measured total thickness 1.7 m, resulting in an overestimation of sea-ice thickness on the order of a factor 2. Our results also highlight the importance of year-to-year regional scale information about the depth and density of the snowpack, as this influences the sea-ice freeboard, the radar penetration, and is a key component of the hydrostatic balance equations used to convert radar freeboard to sea-ice thickness.

Key Points:
- In the N-ICE2015 study region, freeboard retrievals from airborne and satellite radar altimeters are close to the snow freeboard
- Radar penetration in snow can be low even at low temperatures, with consequences for radar-based sea-ice thickness and mass estimates
- In our region treating radar freeboard as sea-ice freeboard results in a sea-ice thickness double that measured in the field

Correspondence to:
H. Skourup,
hsk@space.dtu.dk

Citation:
King, J., Skourup, H., Hvidegaard, S. M., Rösel, A., Gerland, S., Spreen, G., . . . Liston, G. E. (2018). Comparison of freeboard retrieval and ice thickness calculation from ALS, ASIRAS, and CryoSat-2 in the Norwegian Arctic to field measurements made during the N-ICE2015 expedition. *Journal of Geophysical Research: Oceans*, *123*, 1123–1141. https://doi.org/10.1002/2017JC013233

Received 10 JUL 2017
Accepted 18 JAN 2018
Accepted article online 25 JAN 2018
Published online 9 FEB 2018

1. Introduction

A decline in sea ice extent and thickness in the Arctic has been the subject of much concern in recent years (Cavalieri & Parkinson, 2012; Comiso et al., 2008; Kwok & Cunningham, 2015; Kwok & Rothrock, 2009; Meier et al., 2014), fueled by evidence of a transition from a regime dominated by multiyear ice (MYI), to one dominated by seasonal or first-year ice (FYI) (Comiso, 2012). Thinning has been demonstrated using in situ measurements, airborne instruments, submarines, and Upward Looking Sonars (ULS) deployed on moorings (Haas et al., 2008; Hansen et al., 2013; Kwok & Rothrock, 2009; Renner et al., 2013). However, on an Arctic wide scale, satellite data are necessary to get the full picture. Both radar (ERS-1/2, Envisat, CryoSat-2, Sentinel-3, SARAL/AltiKa) and laser (ICESat) altimetry missions capable of polar observations have been launched for more than 25 years (Farrell et al., 2009; Laxon et al., 2013; Wingham et al., 2006; Zwally et al., 2002). CryoSat-2, carrying a Ku-band Synthetic Aperture Interferometric Radar ALtimeter (SIRAL), was launched in 2010, with an orbit designed to take it to 88°N, giving greater coverage of the Arctic Ocean than previous missions (Envisat, ERS-1/2, reaching 81.5°N, ICESat 86°N). The primary objective of the CryoSat-2 mission was to observe the fluctuation in Earth's marine and terrestrial ice sheets over a 3 year period, an objective which the mission has now surpassed.

Sea-ice freeboard is the height of the ice surface relative to the water surface and can be negative if the ice surface is suppressed below the water surface (e.g., if a heavy snow load is weighing down the ice floe). Snow freeboard is the height of the snow surface above the water surface (the sea-ice freeboard plus the snow depth). Ice thickness can be calculated from freeboard or snow freeboard assuming hydrostatic

equilibrium. Laser altimeters, operating in the near-infrared, measure snow freeboard if snow is present because the laser signal is reflected from the snow surface and does not penetrate. For Ku-band radar altimeters, the conventional processing method aims to identify the return from the sea-ice surface producing a radar freeboard that is as close as possible to the sea-ice freeboard. Radar freeboard is identified by a process known as retracking, which aims to identify the mean elevation of the main scattering horizon from a waveform which is an integral of backscatter from the snow surface/volume and the ice surface (Kurtz et al., 2014; Ricker et al., 2014). To be certain the thickness calculated from radar, freeboard is accurate one must be certain that the radar freeboard is at or close to the snow-ice interface. However, questions remain about the accuracy of this process and its impact on the subsequent calculation of ice thickness and the basin-scale sea-ice mass and volume.

A detailed quantification of the contributions to the error budget associated with freeboard retrieval from CryoSat-2 from different sources has been made by the ESA CryoVal-SI project team and summarized in Haas et al. (2016). One of the largest contributions to the error budget is whether the main scattering horizon is at the snow-ice interface or somewhere in the overlying snowpack. When a snow cover is present one cannot be certain that the radar freeboard is at the ice surface because of the interaction between the contributions to the radar returns from the snowpack and sea-ice surface (Gerland et al., 2012; Ricker et al., 2014, 2015). While Beaven et al. (1995) are often cited as showing that radar signal will penetrate through the snow pack to the ice surface under cold, dry, snow conditions; later work by Willatt et al. (2010, 2011), Giles and Hvidegaard (2006), Kwok (2014), and Ricker et al. (2015) demonstrates that it is possible for snow moisture content and density layering to reduce radar penetration.

Another contributor to the uncertainty in the conversion of freeboard to sea-ice thickness is the snow depth and snow and ice densities used in this calculation. Traditionally the snow depth and density values are based on the so-called "Warren climatology" (hereafter referred to as W99), the most comprehensive analysis of measured snow depth in the Arctic available to date, from in situ measurements made at drift stations and airplane landings between 1954 and 1991 (Warren et al., 1999). It has been suggested that in recent years this climatology may be out-dated for some regions, particularly where FYI has become the predominant ice type (Gerland et al., 2012; Kern et al., 2015; Kurtz et al., 2013; Kurtz & Farrell, 2011; Newman et al., 2014; Tilling et al., 2015, 2016; Webster et al., 2014). The use of a snow climatology is also problematic in regions with a high interannual variability. The freeboard to thickness conversion is also sensitive to the density of the ice, in particular to the density difference between first-year and multiyear ice (Kern et al., 2015).

In this paper, we present a data set comprising in situ data (ice and snow depth, snow characteristics), helicopter-borne total (ice plus snow depth) thickness sounding, airborne ALS snow freeboard and ASIRAS radar freeboard, and satellite (CryoSat-2) radar freeboard data acquired during the N-ICE2015 expedition in spring 2015. We first examine the relationship between snow depth and ice and snow freeboard by comparing gridded in situ snow depth measurements with colocated snow freeboard from the ALS. We then move to the intercomparison of freeboards from laser (ALS) and radar (ASIRAS and CryoSat-2) to investigate the penetration of the radar signal into the snow layer. We also compare total thickness calculated from ALS, ASIRAS, and CryoSat-2 with total thickness measurements made with the helicopter-borne electromagnetic sea-ice thickness sounding instrument (henceforth referred to as HEM). We examine the effect of using different snow depth and snow and ice density values, in the conversion of freeboard to thickness. We also investigate whether we can improve the accuracy of the freeboard retrieval from CryoSat-2 by changing the threshold used in the retracking process. We examine the merits of adjusting the retracking threshold in a quest for an accurate sea-ice freeboard versus treating the radar freeboard as snow freeboard. In the discussion we consider how the properties of the snowpack could influence the radar freeboard measured by both ASIRAS and CryoSat-2 in the study area.

1.1. Study Area

This study is located in the Arctic Ocean, in the region north of Svalbard. All data were acquired in April and May 2015 as part of the Norwegian young sea ICE expedition (N-ICE2015) an international project led by the Norwegian Polar Institute (NPI) (Granskog et al., 2016). N-ICE2015 was a drift study in which the research vessel RV Lance was frozen into the ice adjacent to a chosen sea-ice floe to facilitate a comprehensive program of measurements covering the complete atmosphere-ice-ocean system. The location of the drift track

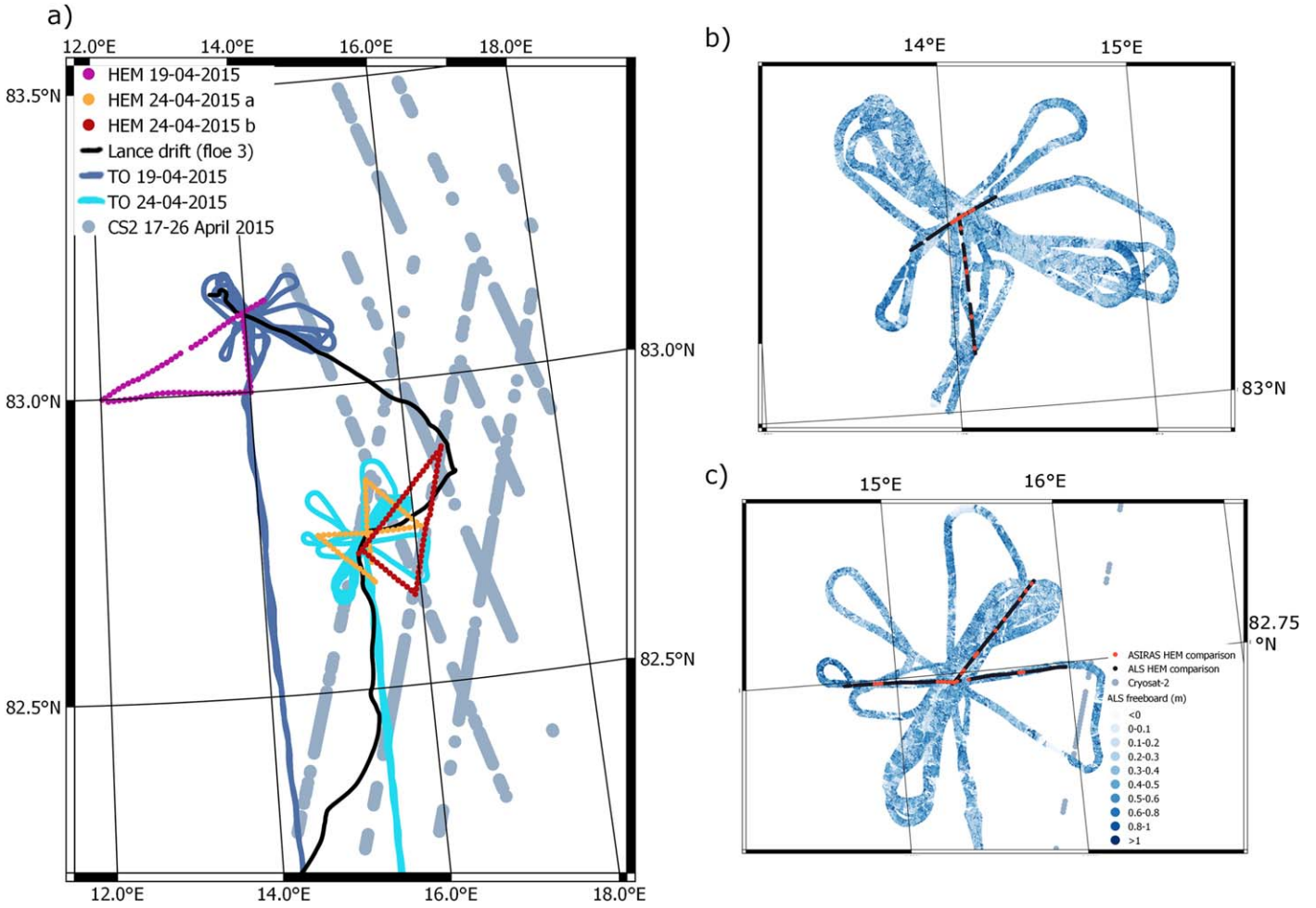

Figure 1. Map showing (a) location of flights and CryoSat-2 overpasses, and the drift track of RV Lance between 19 and 24 April 2015 at Floe 3 of the N-ICE2015 expedition, (b) regions where it was possible to make a direct comparison of HEM to ALS (black lines) and ASIRAS (red lines) for (b) 19 April and (c) 24 April.

of RV Lance within the study region is shown in Figure 1a along with the location of Twin Otter aircraft and helicopter flights and CryoSat-2 satellite orbits on the two key dates from which data is used in this study.

2. Data and Methods

Here we focus first on data collected during two overflights (19 and 24 April 2015) by the British Antarctic Survey (BAS) Twin Otter (TO) aircraft of the N-ICE2015 drift station "Floe 3," as part of EU FP7 program Ice, Climate, Economics, Arctic Research on Change (ICE-ARC). The TO was equipped with the Airborne Synthetic Aperture and Interferometric Radar Altimeter System (ASIRAS), which is an airborne version of the SIRAL radar altimeter on board CryoSat-2 (Borisch, 2011), and an Airborne Laser Scanner (ALS). A helicopter (AS350) based on RV Lance flew part of the same flight lines with the HEM instrument. The dates and times of the flights involved are described in Table 1. In situ data including local area surveys for ice and snow depth (Rösel et al., 2016a, 2016b) and point measurements of snow and ice thickness, density, and stratigraphy (Gerland et al., 2017; Merkouriadi et al., 2017; Rösel & King, 2017) collected on the same dates are used to aid the interpretation of the data from these airborne instruments. In addition we compare the ASIRAS and ALS freeboard to freeboard retrieved from CryoSat-2 during the same period. In sections 3.3 and 3.4, we expand our focus to make a regional comparison of Cryosat-2 freeboard and conversion to sea-ice thickness with all HEM flights (totaling 16) from the campaign (King et al., 2016).

Table 1
Flight Information for Airborne Data Used in This Study

Date	Platform	Instrument(s)	Start time (UTC)	Stop time (UTC)
19 Apr 2016	TO	ALS, ASIRAS	09:42	15:06
19 Apr 2016	AS350	HEM	08:52	10:12
24 Apr 2016	TO	ALS, ASIRAS	09:29	14:42
24 Apr 2016	AS350 (flight a)	HEM	08:46	10:07
24 Apr 2016	AS350 (flight b)	HEM	14:24	15:27

Note. The two platforms are the Twin Otter air craft and the AS350 helicopter.

2.1. In Situ Data

Ice thickness was measured by drilling and with ground-based electromagnetic sounding. Snow depth surveys were made with a GPS snow probe, and detailed studies of were snow characteristics made on each of the days when colocated TO and HEM flights took place. For a more detailed description of the methods used in the ice and snow depth surveys, see Rösel et al. (2018), for a detailed description of the snow characteristics at "Floe 3" see Gallet et al. (2017). Analysis of ice cores for salinity and $\delta^{18}O$ confirms that the ice in the vicinity of RV Lance at "Floe 3" was a mixture of FYI and second year ice (SYI) (Granskog et al., 2017). Back trajectories for the floe show that the SYI originates from the northern Laptev Sea (Itkin et al., 2017).

Twenty-one point measurements of ice thickness, snow depth, and ice freeboard were made by drilling in the days surrounding the two overflights (17–26 April 2015). The measured ice freeboard was between −0.17 and 0.15 m with mean 0 m. Ice thickness was between 0.81 and 2.70 m, with mean 1.49 m; and snow depth between 0.13 and 1.12 m with mean 0.48 m (Rösel & King, 2017).

On the 19 April, an on-ice survey grid was laid out close to RV Lance, which was overflown by both airborne platforms. The survey grid was 400 m × 60 m. Within the grid, total thickness was measured by electromagnetic sounding (EM31, Geonics, Mississauga, Canada; Haas et al., 1997), and snow depth with a GPS snow probe, known as the "MagnaProbe (MP)" (Snow-Hydro, Fairbanks, Alaska). The survey pattern within the grid took the form of a "snake" which crossed from long edge to long edge every 5 m. Total thickness and snow depth measurements were also made on 24 April, on a different (less comprehensive) survey line approximately 100 m apart from the first. The mean and mode of the total thickness from EM31 survey on 19 April are 1.70 and 1.50 m. On the 24 April, the total thickness distribution has mode 2.10 m and mean 2.20 m (Rösel et al., 2016a, 2018).

The mean and mode snow depth on 19 April were 0.40 m. On 24 April, snow depth had mean 0.56 m and mode 0.50 m (Rösel et al., 2016b, 2018). The mean of all snow depth data from both surveys was 0.42 m. The combined mode was 0.40 m. As the surveys took place in different locations using the combined mean is more representative of the general area than using one or the other in the calculations that follow.

Snowpits were dug on 19 and 24 April (Gallet et al., 2017; Merkouriadi et al., 2017). Both snowpits were dug on level SYI. The total depth of the snowpit on 19 April was 0.63 m and on 24 April 0.60 m. As well as measuring snow temperature and density profiles, the snow grain size, and type was characterized, and any ice layers, snow-ice, or slush were recorded. The data are presented in Table 2. On 19 April, the air temperature at 1 m above the surface was −15°C at the snow/air interface −16°C and at the snow/ice interface −6.7°C. On 24 April, these temperatures were −17°C, −15°C, and −6.2°C, respectively. The bulk density of the snow for the specific dates of the two flights is 365 kg m^{-3} on 19 April and 283 kg m^{-3} on 24 April. Instead of taking these measurements from individual snowpits, which only represent one point, the snow density used for the conversion of freeboard to ice thickness in sections 3.3 and 3.5 is the mean of all snow density measurements in snowpits dug on "floe 3" between 19 April and 13 May. Between these dates, temperatures measured in the snowpits remained below −2°C in all layers, while air temperature was between −10°C and −25°C, so we can be confident that changes in density due to thaw and refreezing have not occurred. This regional bulk density is 313 kg m^{-3}. "Slush" layers in the base of the snowpack with density above 500 kg m^{-3} were not included in this calculation. Our measured snow density is not much different from the Warren climatology (320 kg m^{-3}) for the region. This is slightly lower than the mean density of snow on FYI (324 kg m^{-3}) given in Alexandrov et al. (2010), and within the range given by the same for

Table 2
Snowpit Data

Layer number	Depth from bottom (cm)	Temperature °C	Grain size min (mm)	Grain size max (mm)	Hardness	Snow type	Density (kg m^{-3})	SWE (mm)	Thickness of layer (cm)	Comments
19 Apr 2016										
1	63	−15.52	0.1	0.5	4	Windslab	370	22.2	6	
1	58	−15.63	0.1	0.5	4	Windslab	370	18.5	5	Crust at 49 cm
2	51	−14.7	1	2	3	Fragmented	260	7.8	3	
3	48	−14.4	0.5	2	3	Fragmented	300	12	4	
4	43	−12.23	1	3	3	Facetted	310	12.4	4	
5	20	−7.63	4	6	3	Facetted	290	95.7	33	
6	4	−6.75	0.5	2	3	Slush	770	61.6	8	
24 Apr 2016										
1	60	−14.5	0.2	1	1	Fragmented	235	2.35	1	
2	53	−13.99	0.5	1.5	2	Facetted	235	16.45	7	Crust at 59 cm
3	49	−12.89	0.5	1	3	Fragmented	200	10	5	
4	41	−11.07	1	3	1	Facetted	300	9	3	
5	15	−8.08	0.2	1	4	Facetted	300	12	4	
6	2	−6.39	1	3	2	Facetted	300	120	40	

Note. Hardness is defined from very low (1) to very high (5) and snow type described as in Gallet et al. (2017).

snow on MYI. Our mean snow depth (0.34 m) is 8 cm deeper than that of the Warren climatology for the region.

A limited number of sea-ice density measurements are available from ice cores drilled at different locations in the vicinity of RV Lance on 28 April and 12, 14, and 28 May (Gerland et al., 2017). The bulk density of ice in these cores was between 863 and 907 kg m^{-3} representing a mix of MYI and FYI, with an outlier of very compact, deformed MYI, that had bulk density 921 kg m^{-3}.

Air temperature was recorded by a weather station mounted on RV Lance and by a 10 m mast located on the ice approximately 400 m from the ship (Cohen et al., 2017; Hudson et al., 2015). The air temperature between the 19 and 24 April was between −13°C and −25°C.

2.2. Temperature and Precipitation History of the Floe

A drift retrieval algorithm (Itkin et al., 2017) was used to derive a back trajectory for the floe from the merged ASCAT/SSMI sea-ice drift data set (Girard-Ardhuin & Ezraty, 2012). Ice drift from a coupled ocean-sea-ice model (MITgcm ECCO2, 4.5 km grid; Spreen et al., 2016) was used to bridge the summer months. The back tracking algorithm does not consider new ice growth, i.e., the presented trajectories represent the oldest ice for a particular region of about 62.5 × 62.5 km^2.

Having identified the drift trajectory taken by the floe, we use the positions to locate the floe at a given time within the ERA interim reanalysis (Berrisford et al., 2011) data grid cell in order to identify the temperature and precipitation data for that time. The temperature and precipitation history of the floe from July 2014 up to and including the time at which the N-ICE2015 established the research based on the floe in April 2015 are shown in Figure 2.

2.3. HEM Sea-Ice Thickness

A helicopter (Eurocopter AS350) based on RV Lance carried out 16 flights with the HEM instrument between 15 April and 18 May (King et al., 2016). There was one flight with the HEM instrument on the 19 April (pink in Figure 1) and two flights on 24 April (a and b, orange and red in Figure 1), parts of which were colocated with the TO overflights. Flight "b" on 24 April also included a section of direct underflight of CryoSat-2 orbit. Another CryoSat-2 orbit underflight was made on 5 May, which is included in the CryoSat-2 intercomparison study (section 3.3.2). HEM ice thickness measurements are based on the retrieval of the height of the EM instrument above the interface between the resistive sea ice and the conductive seawater, i.e., the height above the bottom of the ice, by electromagnetic induction in the conductive water under the ice. The height of the instrument above the surface of the ice or snow is determined with a laser altimeter included in the EM instrument (Haas et al., 2009). The difference between the two height measurements corresponds

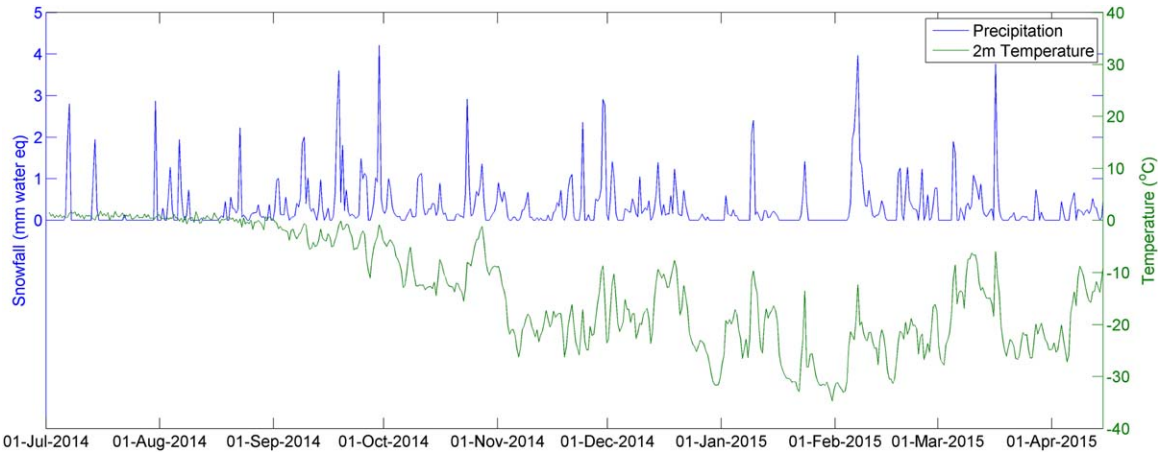

Figure 2. Temperature and precipitation history (ERA reanalysis) of the floe on which in situ measurements were made.

to the total thickness of ice and snow. The nominal ice thickness uncertainty for a single HEM measurement is 0.1 m over level ice, with significantly larger errors and an underestimation of maximum thickness occurring in heavily ridged areas due to footprint smoothing (Haas et al., 2009; Mahoney et al., 2015). Typical HEM footprint size is on the order of 40–50 m. Mean total thickness is 2.06 ± 0.84 m on 19 April, and 1.66 ± 0.85 m for flight (a) and 1.84 ± 0.97 m for flight (b) on 24 April.

2.4. Twin Otter Flights

BAS and DTU Space coordinated six airborne survey flights between 16 and 24 April 2015 north of Svalbard, over Fram Strait, and northeast Greenland. Two of these flights were dedicated to map the sea ice in the area near RV Lance with ASIRAS and ALS altimetry; these flight tracks are shown in Figure 1a in two shades of blue.

2.4.1. Airborne Laser Scanner

The ALS is an airborne laser scanner of type RIEGL LMS-Q240i-80 operating with wavelength 904 nm. The ALS range data have been combined with precise GPS positioning and inertial navigation attitude information to determine the three-dimensional point cloud of the surface. Typical resolution of the raw data is approximately 1 m × 1 m in a 400 m wide swath at the nominal flight altitude of 300 m, and the vertical accuracy is in the order of 0.1 m depending primarily on uncertainties in the kinematic GPS solutions. The point to point shot accuracy of the ALS is 1–2 cm (noise level of laser measurements) and the incidence angle of 0-+-40 degrees limits the return over smooth open water or newly formed smooth ice to angles close to nadir, i.e., no return from most of the swath in these cases. To further obtain freeboard heights, the full resolution data have been thinned in the along-track direction and averaged across-track to a resolution of approximately 5 m × 5 m. Since the laser measures the surface topography, it is crucial to estimate the sea surface height, from which the freeboard heights can be estimated. A geoid model is used as a first approximation of the sea surface height (SSH), and is subtracted from the ALS elevations. Here we have used the most updated version of the Arctic Gravity Project (ArcGP), as the geoid model. Due to SSH variability caused by time varying ocean tides and currents, errors in the ocean mean dynamic topography, and measurement errors, it is necessary to estimate the instantaneously sea surface height by identifying leads in the ice pack. The leads are selected automatically by identifying the minimum values of the orthometric height within equidistant subsections. Typical subsection length is 5 km, which is chosen based on local ice properties and geoid model variations and resolution. As we expect the sea surface to be a smooth surface, minimum points are accepted only if they are within ±0.5 m of a linear fit to the minimum points. The instantaneously sea surface height is estimated by fitting a least-square collocation function to the accepted minimum points. Finally, freeboard heights are found by subtracting the estimated sea surface heights from the thinned and averaged ALS data (see also Hvidegaard & Forsberg, 2002). This method relies on the existence of leads in the ice pack. If the leads are covered by thin ice with or without snow, this will underestimate the sea-ice freeboard heights accordingly (e.g., Kwok & Cunningham, 2008). This, however, is included in the total sea-ice freeboard error estimate (see Hvidegaard & Forsberg, 2002). Manual examination of the data set supports the presence of leads at the 5 km length scale.

2.4.2. ASIRAS

The ASIRAS radar altimeter was operated in low resolution mode (LAMA) at 300 m above ground with a center frequency of 13.5 GHz, a bandwidth of 1 GHz and a pulse repetition rate of 3,000 Hz. The resulting footprint size after SAR processing is approximately 10 m in across-track and 3 m in along-track direction. To estimate the surface elevation, a threshold first maxima retracker (TFMRA) using a threshold of 40% was applied to the processed L1b ASIRAS waveforms. We applied the same retracker to all waveforms to avoid any artificial offsets potentially introduced when applying different retracker algorithms for leads and sea ice waveforms, respectively. The success of this approach has been demonstrated in previous studies (Gerland et al., 2012; Hendricks et al., 2010). The choice of a low threshold on the first maxima reduces the influence of volume scatter on the estimated elevation as has been shown for Cryosat-2 (Helm et al., 2014) and for ASIRAS (Helm et al., 2007). This means that we assume our retracked scattering horizon to be close to the air-snow surface. Therefore, we did not apply any correction for the speed of travel in snow to the measured range.

Because ASIRAS and ALS are measured simultaneously from the same platform, the sea surface height extracted from the ALS data, as described above, has been used as reference sea surface height for ASIRAS to obtain radar freeboard heights. To calibrate the two instruments, manually selected leads have been identified by inspection of aerial images. At the selected leads, it is assumed that the two instruments reflect from the same surface, which is the case for snow free and open water leads. Further, to avoid erroneous surface heights from blurred waveforms, which occurs for large roll angles, a threshold on the roll angle (here $-1.5^\circ < \text{roll} < 1.5^\circ$) is set to remove such erroneous measurements.

2.5. CryoSat-2

The level 1b and 2i (baseline C) ESA CryoSat-2 data were obtained via ftp from science-pds.cryosat.esa.int using the ESA Cryosat User Tool (CUT). All orbits in the region through which RV Lance drifted between 15 April and 18 May 2015 were obtained at both level 1b and 2i. In this region, CryoSat-2 operates in SAR-mode. SAR-mode has footprint size approximately 300 m along-track and 1.6 km across-track. Level 2i data contain a sea-ice freeboard derived using the ESA processor as described in the CryoSat-2 Product Handbook (Bouzinac, 2014). This freeboard is used in the freeboard comparisons made in section 3.2.2 and for the regional experiment with different conversions to ice thickness in section 3.3.3. Data flagged as unreliable are discarded. Level 1b data contain the waveforms from which the freeboard in the level 2i data was derived. To investigate the impact of using different retracking thresholds (see section 2.5.1) on the resulting freeboard (section 3.3.4), we use the waveforms provided in the level 1b data.

2.5.1. Basic Threshold Retracker

Radar freeboard is identified by measuring the travel time of the radar signal from transmitter to receiver, and comparing this to the orbit parameters, height above the geoid or mean sea surface (MSS), and to known open water surfaces. As part of the processing of this radar signal, the main scattering horizon is identified from the radar waveform using a process known as retracking. Our primary CryoSat-2 freeboard data set is the public available ESA L2i product. As the retracker used in the processing chain of the ESA L2i freeboards are currently unknown, we here apply a basic threshold retracker to ESA L1b waveforms to investigate the influence of using different thresholds on the identification of the main scattering horizon. Based on the theoretical analysis, the main scattering horizon for SAR-waveforms is close to 80–90% of the leading edge (Wingham et al., 2004), but are dependent on surface roughness and snow volume scattering. In section 3.3.4, we experiment with thresholds of 50%, 70%, 80%, and 90% of the first maximum of radar echo power. In converting the range identified by the threshold retracker to radar freeboard, we applied the corrections for atmospheric effects and ocean tides that are supplied with the level 1b data. We use the mean sea surface and sea surface height anomaly supplied at level 2i. Using the MSS and local sea surface height anomaly supplied in the L2i data maintains as much as possible the consistency with the ESA freeboard product, i.e., the only variable changed is the retracker, and the retracking threshold. We did not apply our threshold retracker to any waveform where the freeboard was flagged as unreliable in the level 2i data.

2.6. Drift Correction and Colocation of Data

We have identified four sections of the flights made by the two platforms (AS350 and TO), where direct along-track comparison is possible, see Figures 1b and 1c. Because the flights on a given day are separated

in time (Table 1), it is necessary to account for the sea-ice drift that occurred between the two flights in order to colocate them. To account for the sea-ice drift in between the two surveys, both data sets are transferred to the same reference time, at 12:00 UTC of the given day. This is done assuming the sea-ice drifts with the same speed and direction as RV Lance and assuming no significant rotation and deformation of the sea ice. The position of the ship recorded every minute is used and a linear drift is assumed between each position. The ship drift direction changes only slowly during the survey time therefore only small deformation of the ice field is expected. In support of the validity of these assumptions, the overlapping laser scanner data show good agreement after applying the drift correction. The EM31 and MP data are drift-corrected to 12:00 UTC in a similar way,and gridded on a 5 m grid (Rösel et al., 2017).

For the ALS-ASIRAS intercomparison study, see section 3.1, the ALS data points have been correlated with the ASIRAS measurements only where ALS measurements are located within 7.5 m radius of the corresponding ASIRAS measurement, corresponding to the ASIRAS footprint size of 10–15 m.

To make direct along-track comparison of HEM and ALS/ASIRAS, the two data sets have been colocated and averaged to obtain comparable spatial resolution. For each of the HEM observations, the ALS and ASIRAS freeboards are averaged within a search radius of 20 m to match the HEM footprint of 40–50 m, using weighted mean interpolation. In a similar way, the in situ data from EM31 and MP have been compared to ALS by prediction of values coincident with ALS within a 5 m search radius.

In order to enable along-track comparison for the two CryoSat-2 underflights, the HEM data from these flights were regridded onto the CryoSat-2 footprints (300 m × 1,600 m) for the relevant orbits. The mean, mode, and standard deviation of the HEM total thickness were calculated for each footprint following the method described in Haas et al. (2016).

2.7. Conversion of Freeboard to Thickness

The conversion of the measured freeboard h_f to sea-ice thickness h_i relies upon the hydrostatic balance equation, and is dependent on whether one uses sea-ice or snow freeboard. For radar altimetry, following the assumption that the radar freeboard is equal to the ice freeboard, equation (1) (Forsström et al., 2011) is valid. We use density of sea water ρ_w 1,025 kg m^{-3}; for ice density ρ_i, we use 882 kg m^{-3}. This value is often used in the literature to represent MYI (Kwok & Cunningham, 2015) and falls within the range of density measured in the field on both MYI and FIY. In support of this choice we experimented also with FYI density 917 kg m^{-3} and found that in all cases using the MYI density produced mean thickness slightly closer to that measured in the field. To reduce the number of variables considered, we present in the following sections only results using the MYI density.

For snow density ρ_s and snow depth h_s, we can use the mean values from our field measurements: 313 kg m^{-3} and 0.42 m, respectively (see section 2.1). In section 3, we compare results when we use our snow observations defined by the field data to results produced from the use of both W99 and the so-called "half-W99," often applied in regions of FYI, where the snow depth from W99 is halved but the density remains the same:

$$h_i = \frac{\rho_w}{\rho_w - \rho_i} h_{fice} + \frac{\rho_s}{\rho_w - \rho_i} h_s \tag{1}$$

To convert snow freeboard to sea-ice thickness, we use two different approaches. The first uses equations (2) and (3) following the ESA CCI approach described in Kern et al. (2016). Equation (2) is for the case where the measured snow freeboard is greater than the snow depth. Equation (3) is for the case where the opposite is the case, i.e., snow depth is greater than measured snow freeboard resulting in negative ice freeboard. This case assumes that slush has formed at the base of the snowpack due to water incursion as a result of negative freeboard, and that the density of the slush is equivalent to the density of the ice:

$$h_i = \frac{\rho_w}{\rho_w - \rho_i} h_{fsnow} + \frac{\rho_s - \rho_w}{\rho_w - \rho_i} h_s \tag{2}$$

$$h_i = \frac{\rho_s}{\rho_w - \rho_i} h_{fsnow} \tag{3}$$

The second approach is the "modified ice density" method, also described in Kern et al. (2016), where the modified ice density ρ_i* can be defined:

$$\rho_i * = \frac{h_i\rho_i + h_s\rho_s}{h_i + h_s} \tag{4}$$

This modified density is a bulk density of ice and snow together. Ice thickness can then be calculated using the modified density and snow freeboard following:

$$h_i = \frac{\rho_w}{\rho_w - \rho_i *} h_{fsnow} \tag{5}$$

Using the modified density method can help to avoid problems associated with negative freeboard.

Equations (1)–(5) are all related with uncertainties due to uncertainties in the freeboards, snow depth, and snow, ice, and water densities. Estimates of the radar freeboard (equation (1)) and the snow freeboard (equation (2)) are given in Giles et al. (2007) and read 0.46 and 0.76 m, respectively. Equations (3)–(5) are expected to be associated with uncertainties of the same order.

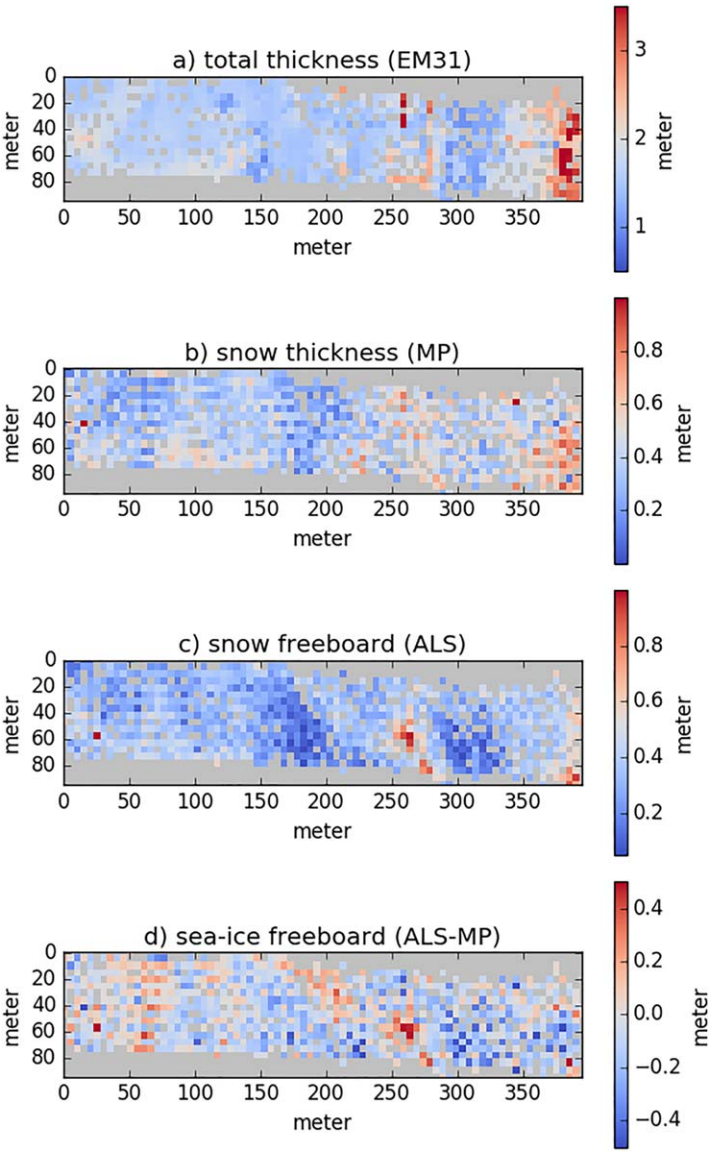

Figure 3. Comparison of total thickness (EM31) and snow depth (MP) to snow freeboard (ALS), with the sea-ice freeboard calculated from snow freeboard-snow depth. The grid spacing is 5 m × 5 m.

3. Results

3.1. Comparison of In Situ Snow Depth Data From the Detailed Survey on 19 April to ALS Freeboard

We compare the measured total thickness (EM31; Figure 3a), and snow depth (MP; Figure 3b), to the snow freeboard (ALS; Figure 3c). We then calculate sea-ice freeboard from the ALS snow freeboard and MP snow depth (Figure 3d) showing that for at least half of the survey grid the sea-ice freeboard is negative. The snow depth on the survey grid has mode 0.45 m and mean 0.37 ±0.15 m, while the snow freeboard has mode 0.30 m and mean 0.32 ±0.13 m. The mean difference between the snow depth and the ALS is 0.06 ± 0.21 m, therefore the calculated sea-ice freeboard has mode and mean −0.06 m. This is within the range of the freeboard measured at drill holes. It is unfortunately not possible to compare the ASIRAS data to the in situ data in the same way because the foot print spacing is such that only a limited number of (valid) ASIRAS freeboards are located within the survey grid. However, due to the high bandwidth of ASIRAS, we were able to clearly define two interfaces in the radargram across the validation site (Figure 4). Visible in this radargram is some layering, a lead and a ridge. The dotted line is the surface retracked with TFMRA. Clearly visible, the retracked surface is located in the leading edge of the waveform and therefore before the first maximum. We assume the two interfaces are the air/snow and snow/ice interface giving additional confidence that the TFMRA retracked elevation is close to the snow surface. The elevation on the *y* axis in this plot is calculated using light velocity (3×10^8 m s^{-1}). To use the difference between the surface and deeper layer as a proxy for the snow depth, one must use the bulk density of 313 kg m^{-3} measured in the field to adjust the velocity. This means that a 1 m difference in the plot reduces to approximately 0.79 m for the final snow depth, therefore in the region shown the snow depth would be between approximately 0.4–0.7 m based on ASIRAS data.

3.2. Penetration Depth—Comparison of ALS, ASIRAS, and Cryosat-2 Freeboard Retrievals

3.2.1. ALS Versus ASIRAS

The ALS-ASIRAS comparison is made for a region within a radius of 50 km of RV Lance to include a larger amount of data to compare to CryoSat-2. This region does not include the part of the TO flight over the marginal ice zone on the way to and from the location of RV

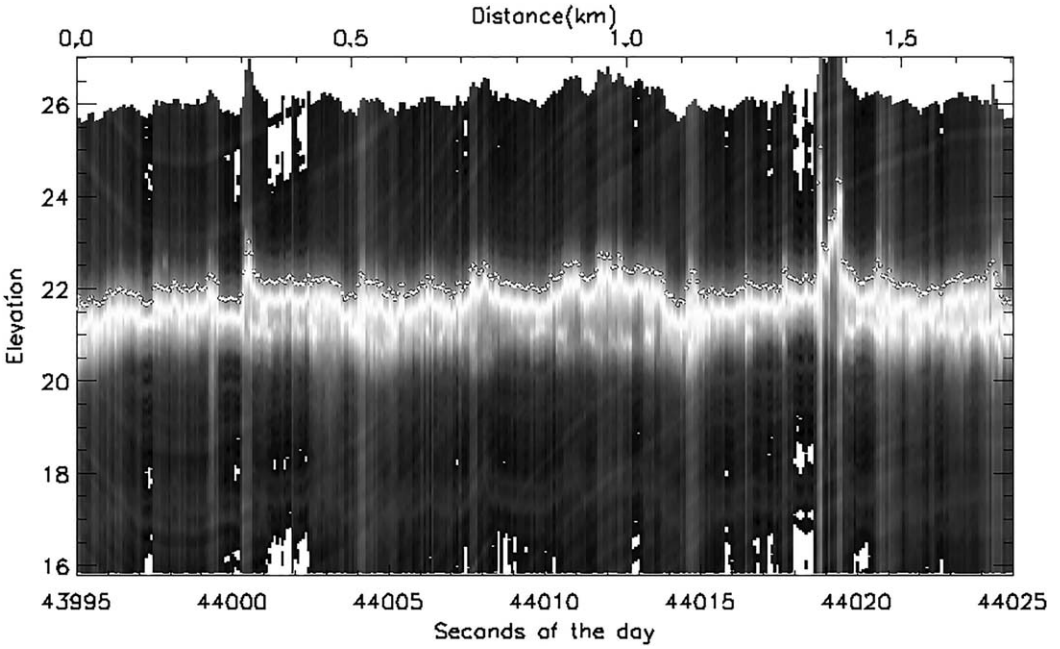

Figure 4. Radargram located within 10 m of the ground survey grid used on 19 April. Visible in this radargram is some layering, a lead and a ridge. The dotted line is the surface retracked with TFMRA. Clearly visible, it is located in the leading edge of the waveform before the first maximum.

Lance. The correlation coefficient between ALS freeboard and ASIRAS freeboard is 0.87 with RMSE 0.15 m on both 19 and 24 April (see Table 3 and Figure 5). The difference between the mean ASIRAS freeboard and mean ALS freeboard is only 3–4 cm on both days, with ASIRAS freeboard lower than the ALS freeboard (Table 4).

3.2.2. Regional Comparison Including CryoSat-2

A regional comparison of the freeboard supplied in the ESA L2i (Baseline C) CryoSat-2 product, to the ASIRAS and ALS freeboards within a radius of 50 km of RV Lance on the 19 and 24 April 2015, is shown in Figure 6. For this regional comparison, we use CryoSat-2 data from 48 h either side of the date on which TO and AS350 flights took place and field data were collected. This was done in order to achieve a better regional coverage; i.e., for comparison with the flight on 19 April we took all CryoSat-2 orbits in the region between 17 and 21 April and for comparison with the flight on 24 April we took all between 22 and 26 April. Orbit locations are marked in Figure 1. On the 19 April, the ALS mean is 0.39 m while the ASIRAS and CryoSat-2 both have mean freeboard of 0.35 m. On the 24 April, the mean freeboards for all three are also in close agreement at 0.40, 0.38, and 0.41 m (Table 4).

3.3. Comparison of HEM to Ice Thickness Calculated From ALS, ASIRAS, and Cryosat-2

The HEM instrument was not flown on the same platform as ALS and ASIRAS; therefore, the area for which a direct comparison between them can be made is more limited than for the ALS versus ASIRAS comparison above. Due to the different geometry, look angle, and measurement pattern of the ALS and ASIRAS instruments, the overlap with HEM data is different for the two instruments (see section 2.4). There are four along-track sections where it is possible to make a direct comparison between ALS and HEM, with short parts of these sections where there are also valid ASIRAS freeboards, see Figures 1b and 1c. The correlation between HEM total thickness and ALS freeboard is 0.74 on 19 April and 0.70 on 24 April; and between HEM and ASIRAS freeboard 0.81 on 19 April and 0.65 on 24 April. The high correlation gives us confidence in the drift correction and colocation of the data.

Table 3
Correlation and RMSE for ALS Versus ASIRAS

Date	19 Apr 2015	24 Apr 2015
Correlation	0.88	0.87
RMSE	0.15	0.15

3.3.1. Along-Track Comparison: HEM Versus ALS

We converted ALS snow freeboard to ice thickness using the ESA CCI and modified density method as described in section 2.7. For the conversion, we use the snow depth and density from our measurements

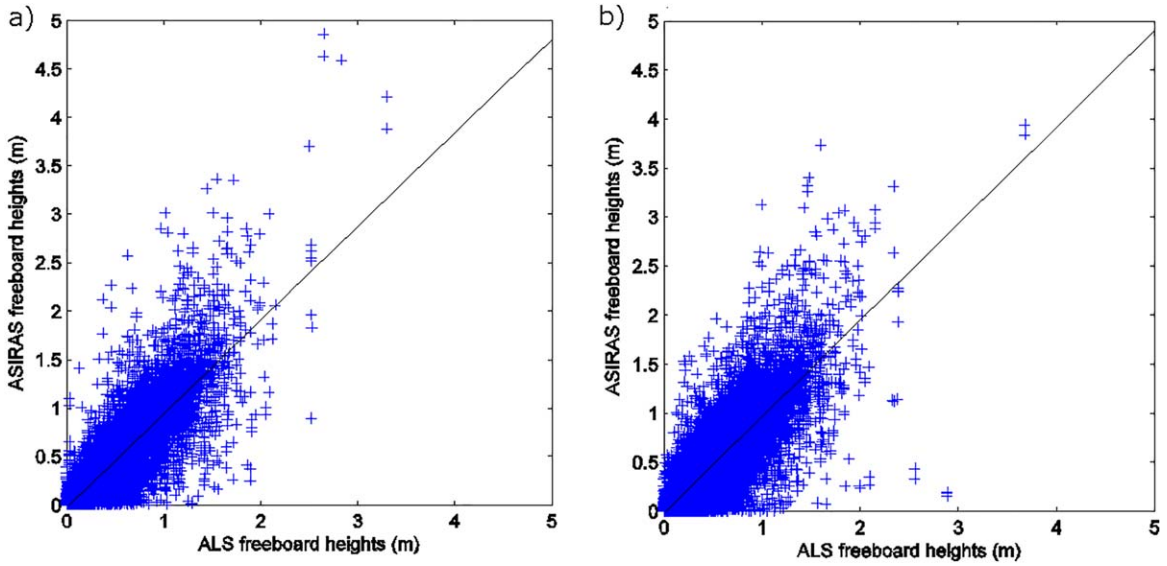

Figure 5. ALS versus ASIRAS freeboard for TO flights on (a) 19 April 2015 and (b) 24 April 2015.

in the field and MYI density. To finally obtain the total thickness (sea-ice plus snow), as obtained by HEM, we added the mean snow depth (0.42 m) from the in situ measurements to the calculated ALS ice thickness. The result from the modified density method has slightly better correlation to HEM than that from the ESA CCI method (Table 5). Total thickness derived using this approach has correlation with HEM 0.74 on 19 April and 0.71 on 24 April with RMSE 0.64 m and 0.69 m. As seen in Figure 7, the ALS retrieves thicker ice in areas with thick ice, when compared to HEM thicknesses. This is expected as HEM tends to underestimate thick and deformed ice (see, e.g., Haas et al., 2009; Mahoney et al., 2015). The mean total thickness calculated from ALS using the modified density approach is 1.41 $\pm$ 0.86 m on 19 April and 1.49 $\pm$ 0.91 m on 24 April, compared to total thickness of 2.06 $\pm$ 0.84 m and 1.76 $\pm$ 0.92 m for HEM. The difference between our calculated results to the HEM observations might be caused by the uncertainties of the density measurements and/or by the spatial variability of the snow depth.

3.3.2. Along-Track Comparison: HEM Versus ASIRAS

A detailed comparison of thickness from ASIRAS and HEM is more difficult than for ALS because the coincident data coverage is limited. The traditional approach to converting radar freeboard to sea-ice thickness treats radar freeboard as sea-ice freeboard (equation (1) in section 2.7). We try this approach using (a) snow depth and density measured in the field, (b) W99, and (c) half-W99. We keep the ice density constant. The modal thickness calculated using this method with our snow observations is 3.4 m. Using the W99 climatology gives a similar result, while using half-W99 gives a regional mode of 2.8 m. These results are too thick by up to a factor 2 when compared to the total thickness from HEM (Figures 8 and 9). Performing the conversion from radar freeboard to sea-ice thickness by taking radar freeboard to be instead snow freeboard and using the modified density method produces a regional sea-ice thickness distribution very similar to that measured with HEM, with mode 1.4 m (Figure 9). Unsurprisingly given how close the ASIRAS and ALS freeboards are to each other, treating the ASIRAS freeboard as snow freeboard, using the modified density method, produces a lower RMSE when compared with the HEM data (Table 6 and Figure 8). This method produces the best results for ASIRAS total thickness versus HEM total thickness with RMSE 1.07 m on 19 April and 1.09 m on 24 April (Table 6).

Table 4
Comparison of Mean Freeboard From ALS, ASIRAS, and CryoSat-2 Within a 50 km Radius of RV Lance

Section	ALS fb mean (std) (m)	ASIRAS fb mean (std) (m)	CryoSat-2 fb mean (std)
19 Apr 2015	0.39 (0.25)	0.35 (0.28)	0.35 (0.13)
24 Apr 2015	0.40 (0.26)	0.38 (0.29)	0.41 (0.30)

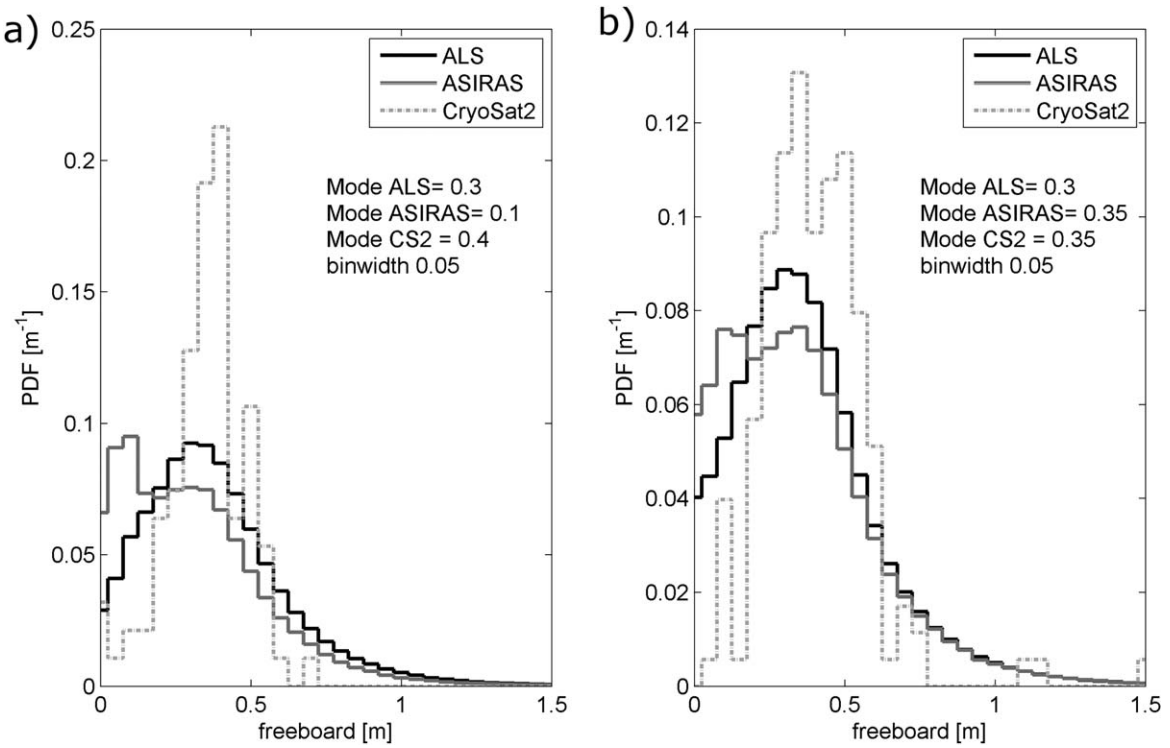

Figure 6. Comparison of freeboard distribution from CryoSat-2, ASIRAS, and ALS on (a) 19 April 2015 and (b) 24 April 2015 (right).

3.3.3. Regional Sea-Ice Thickness From CryoSat-2

In this section, we expand the time frame to consider all CryoSat-2 and HEM data acquired in the region through which RV Lance drifted between 15 April and 19 May. We compute sea-ice thickness from CryoSat-2 using the same methods described in section 2.6. We compare the ice thickness distribution computed from the freeboard in these data to the total thickness distribution from all HEM flights carried out between 15 April and 19 May (Figure 10a). In similarity with the results from ASIRAS presented above, taking radar freeboard as sea-ice freeboard produces a modal thickness significantly above that measured by HEM (the red line in Figure 10a). The modal CryoSat-2 total sea-ice thickness for the region calculated using our snow observations was 3.9 m. Performing the conversion from freeboard to thickness by instead taking radar freeboard as snow freeboard and using the modified density method (see section 2.7) produces a regional CryoSat-2 sea-ice thickness distribution similar to that measured with HEM, with a mode 1.57 m and mean 1.49 m, compared to mode 1.70 m and mean 1.78 m from HEM.

3.3.4. An Experiment With Changing the Retracking Threshold

It is apparent from the above result that the ESA L2i CryoSat-2 freeboards within our study region are dominated by returns from within the snowpack, giving a retracked scattering horizon close to the snow surface, rather than penetrating to the ice surface. In order to determine whether it is possible to derive a radar freeboard close to sea-ice freeboard by changing the retracker threshold, we ran all the CryoSat-2 waveforms from this region through a basic threshold retracker as described in section 2.5.1. The radar freeboard obtained in this way was converted to sea-ice thickness using the values from our snow observations and sea-ice density of MYI. Figure 10b shows the resulting sea-ice thickness distributions with the HEM total thickness distribution for comparison. Using a retracking threshold of 0.5 produces a regional sea-ice thickness mode of 4.8 m. This is slightly higher than that resulting from the use of the radar freeboard supplied with the ESA L2i product. Using a retracking threshold of 0.7 or 0.8 gives an improvement in regional freeboard retrievals and corresponding sea-

Table 5
Correlation and RMSE for Ice Thickness Calculated From ALS Versus Measured Total Thickness (HEM)

Date	19 Apr 2015	24 Apr 2015
Modified density method		
Correlation	0.74	0.71
RMSE	0.64	0.70
Calculated mean thickness (m)	1.41 ± 0.86	1.49 ± 0.91
ESA CCI method		
Correlation	0.67	0.65
RMSE	0.97	0.92
Calculated mean thickness (m)	1.56 ± 1.15	1.68 ± 1.17

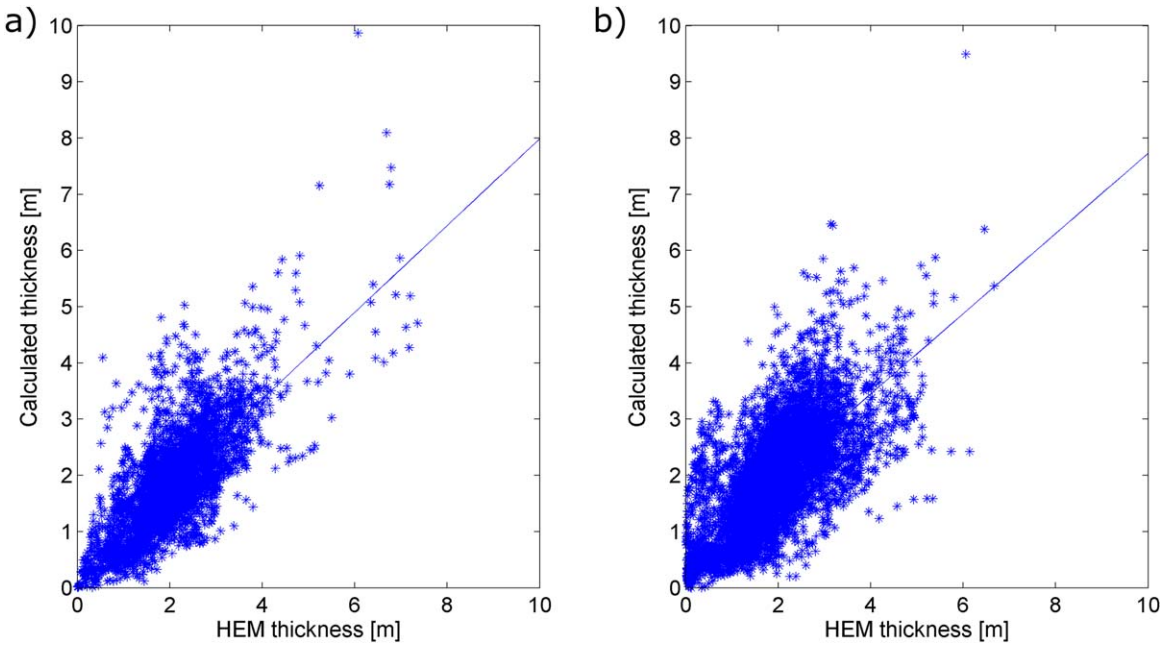

Figure 7. HEM total thickness versus total thickness calculated from ALS using the modified density method (a) 19 April and (b) 24 April. The thickness calculation used MYI density of 882 kg m^{-3} along with the mean snow depth and density from the field measurements.

ice thickness, with mode 2.6 and 1.5 m as expected (see section 2.5.1). However, neither of these thresholds captures the predominance of negative freeboard seen in the field. Only using a threshold of 0.9 results in over 50% negative freeboard retrievals. The width of the CryoSat-2 ice thickness distribution, however, is much wider than what is observed by HEM, independent of the retracker threshold used. None of the thresholds used in this experiment resulted in as good of a match between sea-ice thickness distribution from HEM and CryoSat-2 in this region as was found by treating the L2i freeboard as snow freeboard as described in section 3.3.3.

4. Discussion

In this study, we have shown that the main scattering horizon of ASIRAS using TMFRA and CryoSat-2 L2i freeboards is closer to the ALS snow freeboard than to the sea-ice freeboard observed from drill hole measurements, or the sea-ice freeboard calculated from EM31 and MP transects (sections 3.1 and 3.3.3).

Figure 4 also shows the complexity of the ASIRAS response to sea ice and snow, as at some locations a second layer is seen. The differences between the two layers (0.4–0.7 m) are close to the snow depths found in the in situ data with mean 0.48 m and maximum 1.12 m (see section 2.1). However, Figure 4 only represents a small part of the study area and needs further investigation. A similar layering is not expected to be found in the CryoSat-2 waveforms due to the lower vertical resolution of CryoSat-2 compared to ASIRAS.

The best match between sea-ice thickness distribution from HEM and sea-ice thickness obtained from CryoSat-2 ESA L2i freeboards is by treating the freeboard as snow freeboard. Another threshold can mitigate but not solve the problem (Figure 10), which might be a result of snow volume scattering. We also show that a modified density approach to convert snow freeboard into thicknesses gives the best results in this case, where we have deep snow and widespread negative freeboards.

The measurements obtained by this approach results in mean CryoSat-2 and ASIRAS freeboards in the region between 0.35 and 0.41 m compared to mean ALS snow freeboards of 0.40 and 0.38 m. The measured snow freeboard (from in situ drillings) is between 0.20 and 0.95 m with mean 0.48 m, while the measured sea-ice freeboard was between −0.17 and 0.15 m with a mean of 0 m. We have examined the gridded products made available by NASA (Kurtz & Harbeck, 2017), AWI (Ricker et al., 2014), and CPOM (Laxon et al., 2013), and find that within the same region as used for our analysis in our section 3.3.3. These products

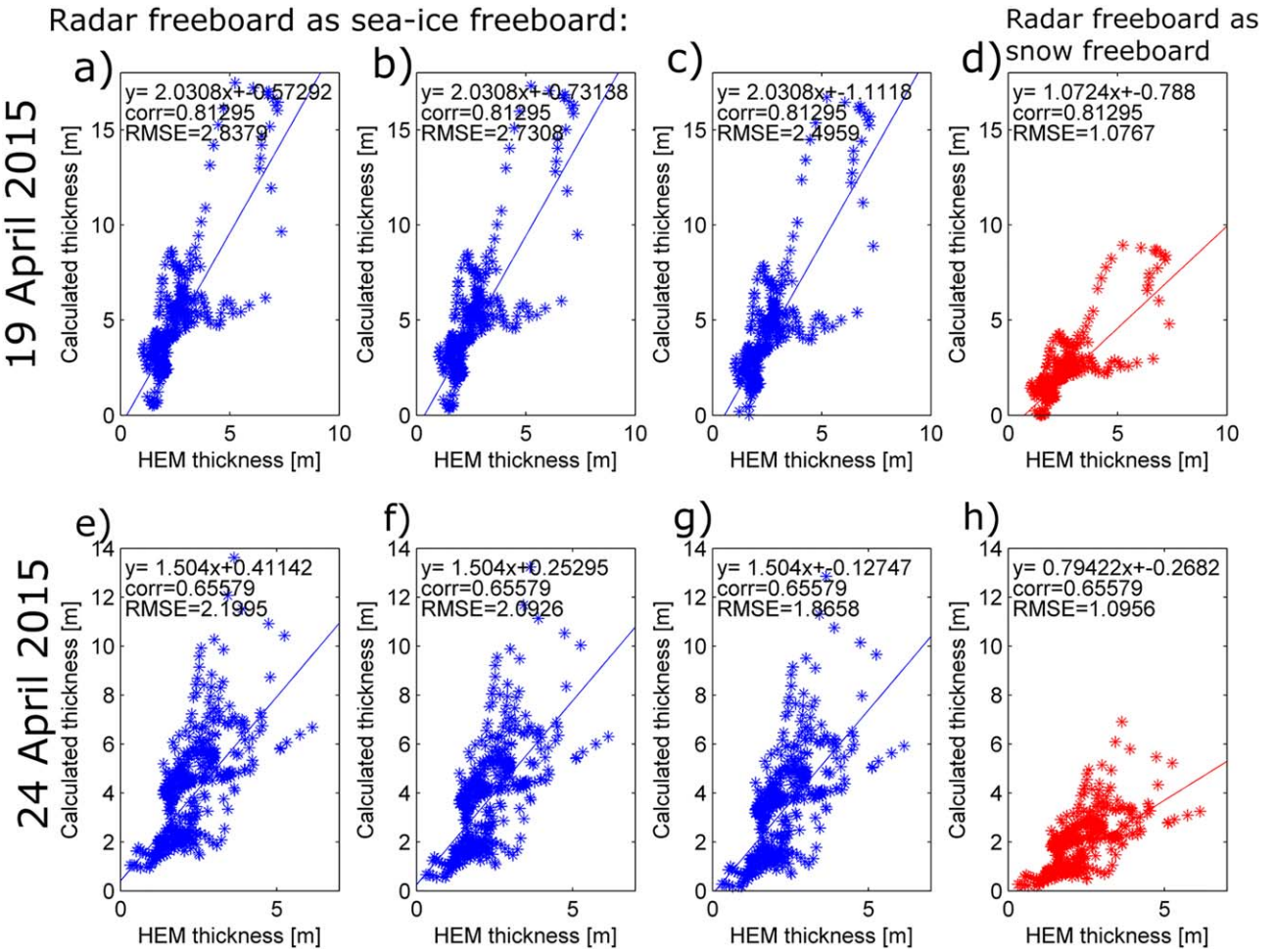

Figure 8. HEM total thickness versus total thickness calculated from ASIRAS taking radar freeboard as sea-ice freeboard and using (a and e) the snow depth and density measured in the field, (b and f) W99, (c and g) half-W99 for snow depth. For comparison in Figures 8d and 8h, the modified density method (which takes radar freeboard as snow freeboard) is used with the snow depth and density measured in the field. The top row is the data from 19 April and the lower row is from 24 April. In all examples MYI density of 882 kg m^{-3} is used.

have a mean sea-ice thickness of 3.16, 3.33, and 3.21 m, respectively. These sea-ice thickness are not consistent with our in situ and HEM measurements. Our results suggest that the overestimated ice thickness in this study region in the NASA/AWI/CPOM data may result from the influence of volume scattering, from the deep snowpack we observed, on the retrieval of radar freeboard.

Previous work has shown that low Ku-band radar penetration in snow is possible at air temperatures above −10°C (Gerland et al., 2012; Giles & Hvidegaard, 2006; Willatt et al., 2011), with the implication being that if the air temperature is high the temperature within the snowpack will approach 0°C, density will increase, and liquid water may be present. With this study, we show that low penetration into the snowpack is also possible at lower air temperatures, down to −25°C.

Snow on sea ice is not a flat homogenous layer. There are several characteristics documented in the snow packs of both days with TO flights that would limit the penetration of the radar signal (Table 2). First, there is slush at the bottom of both snowpits. This is the result of salt water incursion due to the negative freeboard, not to melting within the snow pack. The temperature profiles show that the snowpack was not warm enough for melting to be occurring even at the base (Table 2). Furthermore, there was evidence of ice lenses caused by melt events in early season snowfall close to the base of the snowpack (Gallet et al., 2017). These were only found on the SYI, not on FYI. This is consistent with the temperature history of the floe where the temperature can be seen to rise toward zero in early November (Figure 2), after several early season precipitation events which likely fell as snow. This snow, with melt crust from the warming event, is

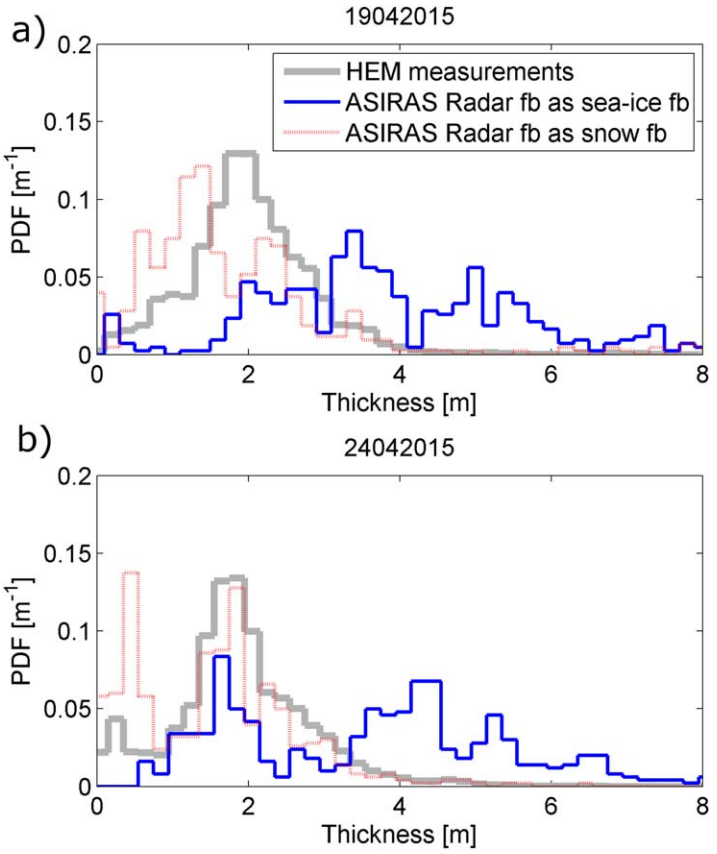

Figure 9. Measured total thickness distribution (HEM) compared to ice thickness distribution calculated from ASIRAS radar freeboard if radar freeboard is taken as sea-ice freeboard (blue line) and as snow freeboard (red line) for (a) 19 April 2015 and (b) 24 April 2015. In all cases, snow depth and density measured in the field and MYI density of 882 kg m^{-3} is used.

Table 6
Correlation and RMSE for Ice Thickness Calculated From ASIRAS Versus Measured Total Thickness (HEM)

Date	19 Apr 2015	24 Apr 2015
Radar fb as sea-ice fb with snow depth and density measured in the field		
Correlation	0.81	0.66
RMSE	2.84	2.20
Radar fb as sea-ice fb with W99		
Correlation	0.83	0.66
RMSE	2.73	2.09
Radar fb as sea-ice fb with half-W99		
Correlation	0.81	0.66
RMSE	2.5	1.87
Radar fb as snow fb		
Correlation	0.81	0.66
RMSE	1.07	1.09

only found on SYI because FYI was not established yet. The slush layer and ice lenses will definitely influence the radar return, possibly masking the return from the sea-ice surface. However, the documented slush layer was only a couple of cm thick, and the ASIRAS radar freeboard has mean 0.35 m on 19 April and 0.38 m on 24 April, while the CryoSat-2 has mean freeboard 0.35 and 0.41 m. Nevertheless, the presence of slush will also increase the salinity of the snow at least several centimeters above the slush top. A recent study (Nandan et al., 2017) shows that even nonflooded snow on FYI in the Canadian Arctic significantly influences the radar signal due to a saline snow pack and shifts the main scattering horizon upward into the snow cover. There is also a wind crust (density unknown) documented at 0.49 m above the snow-ice interface in the snowpit on 19 April and at 0.59 m above the snow-ice interface on the 24 April. Such wind crusts were widespread in the snow on both FYI and SYI (Gallet et al., 2017). It is not possible to identify and isolate radar returns from any individual structure within the snowpack; but it seems clear that the combined impact of these structures on the bulk density and snow water equivalent of the snowpack results in reduced radar penetration. The mean ASIRAS and CryoSat-2 freeboard levels for the region are similar, allowing us to infer that both radars are affected in a similar way by the properties of the snowpack. Theoretical modeling of Ku backscatter properties of the snow may add information to interpretation of the radar return. This is not possible from the information presented here and we recommend this for further study.

We have also shown the effects of using different snow depth and density parameters in the conversion of freeboard to thickness. The W99 climatology is mainly based on measurements made on MYI, although the Sever program (included therein) sampled both FYI and MYI. However, while snow depth in regions dominated by MYI is still quite consistent with the climatology, in regions where FYI has become the predominant this is not the case (Gerland et al., 2012; Kern et al., 2015; Kurtz et al., 2013; Kurtz & Farrell, 2011; Newman et al., 2014; Tilling et al., 2015, 2016; Webster et al., 2014). Accurate satellite radar altimeter estimates of sea-ice thickness require use of the snow properties associated with the most prevalent ice type within the altimeter foot print in the conversion of freeboard to thickness; with far reaching consequences for the total Arctic sea-ice mass and volume calculation if the wrong parameters are used. The study region was marked as FYI in the CryoSat-2 level 2i product but we found that the region contained a mixture of FYI and MYI, that using MYI sea-ice density was more appropriate than FYI sea-ice density, and that our snowpack parameters were closer to W99 than to half-W99. We found on FYI the snow depth expected on MYI. Conversely, work carried out in the same region in 2011 by Gerland et al. (2012) found mainly FYI, on which half-W99 was a more appropriate approximation, because the snow depth was only 0.18 m. Our bulk snow density from all snowpits with cold snow (313 kg m^{-3}) is not very different to the W99 Arctic-wide mean for May, which is 320 kg m^{-3}. In 2011, the measured snow density in the same region was 363 kg m^{-3} (Gerland et al., 2012).

This study highlights the importance of error analysis for basin scale thickness estimates in two ways. First, the study area is located in a different region to the recently published work of Ricker et al. (2015), who also demonstrated low radar penetration in a similarly deep Arctic snowpack. Second, the snowpack found in our study area was shown to be very different to that which one might have expected

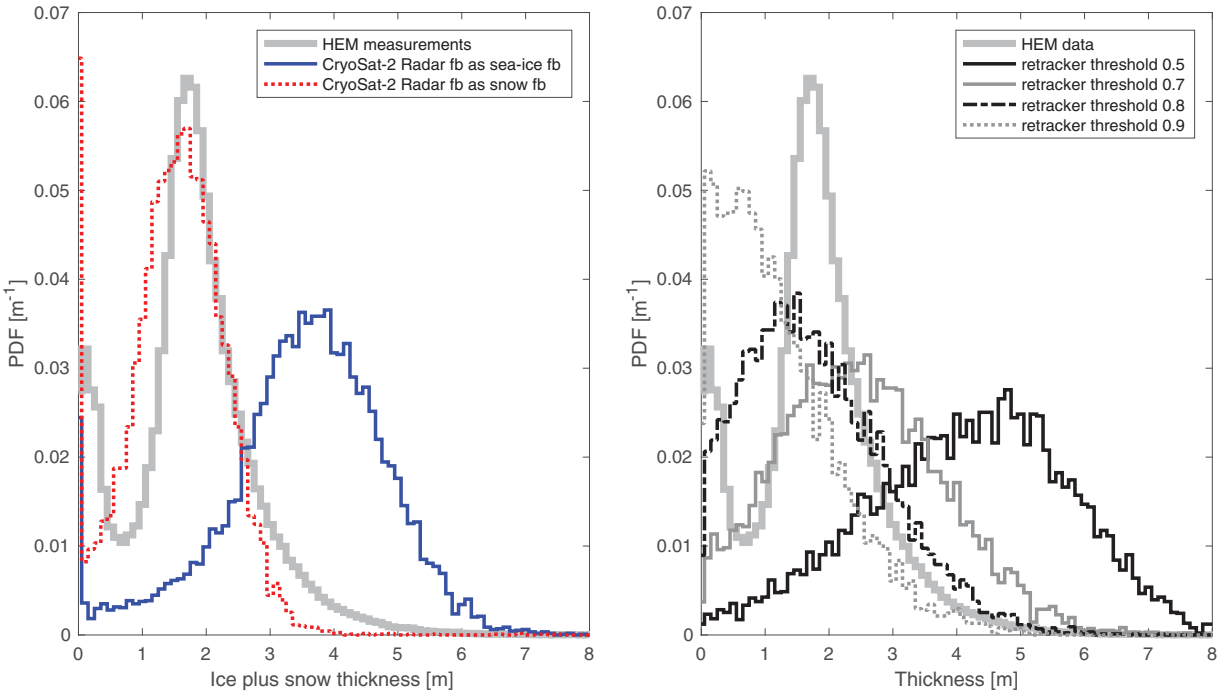

Figure 10. (a) Sea-ice thickness distribution calculated from CryoSat-2 freeboard on a regional scale taking CryoSat-2 radar freeboard as sea-ice freeboard (blue line) and as snow freeboard (red line). (b) Sea-ice thickness distribution calculated from CryoSat-2 from the same region: a comparison of the results from different retracking thresholds. Both with sea-ice thickness distribution from HEM for comparison.

from the W99 climatology. It is important to note that W99 does not include any measurements from our study region. This is a limitation of this climatology, as regional differences and interannual variability are important factors in determining snow depth and density.

If a given error in the conversion of radar freeboard to sea-ice thickness is consistent, and does not change in time and space, then it will have limited impact on the derivation of the trend in sea-ice thickness on a basin scale. However, for the radar penetration depth in snow this is not the case, as shown here and in Gerland et al. (2012) and Ricker et al. (2015). If snow properties change due to interannual variability or climate trends a misinterpretation is possible when data from years with different snow properties are compared. Especially if ice thickness estimates from radar altimetry are combined with those from laser altimetry, these errors can cause biases and artificial trends. Finally if one wishes to use CryoSat-2 to make an accurate assessment of ice thickness in a region at a given time, for example, to provide data for operational purposes, the uncertainties are of course important.

Together this evidence confirms that where a thick snowpack is present it may be necessary to modify the approach to convert radar freeboard to sea-ice thickness. Ricker et al. (2014) suggest that applying different retracker thresholds depending on the seasonal properties of the snow load will be necessary and our results definitely support that. However, Kurtz et al. (2014) show that waveform fitting identifies a scattering horizon closer to the peak than commonly used in threshold retracking, and dispute that a retracker threshold of 50 or even 80% as recommended by Ricker et al. (2014) would necessarily be the ice/snow interface. Following our experiment with the different retracker thresholds in section 3.3.4, we are inclined to agree with this. Furthermore, using a high enough threshold to bring radar freeboard close to the sea-ice freeboard, will, in regions with a heavy snow load on relatively thin ice, result in the identification of a high percentage of negative freeboard, which brings with it a new set of problems in relation to the conversion of freeboard to thickness. The way the equations for hydrostatic equilibrium are formulated assumes that there is a clear boundary between snow and ice. Where negative freeboard is present and flooding is possible this interface is more complex, and may include a slush layer of unknown density.

Because in our study region the radar returns are close to snow freeboard and snow depth is such that negative sea-ice freeboard becomes widespread, we have turned to techniques used to derive sea-ice thickness

in Antarctica where this is a more typical situation. We have demonstrated that under these specific conditions this approach can be quite successful for deriving sea-ice thickness from both ASIRAS and CryoSat-2 radar freeboard. It is likely that this situation will become more common in the Arctic in a warming climate, although the future Arctic snowpack is very uncertain. Snow depth on FYI may increase due to incursions of warm moist air in winter (as opposed to the normal situation of a prevailing high) (Bintanja & Selten, 2014; Graham et al., 2017; Park et al., 2015; Woods & Caballero, 2016). This increase in snow depth, and associated inhibition of ice growth due to the insulating properties of the snow, will promote negative freeboard due to snow falling on ice not thick enough to support it. Conversely it is also possible that delayed ice formation in an Arctic that has moved toward a more seasonal ice cover will result in early season snowfall being "lost" into the sea (Webster et al., 2014).

5. Conclusions

We have presented a data set comprising colocated freeboard and sea-ice and snow depth measurements from point to regional scales in the Norwegian Arctic in late April 2015. We have shown that the main scattering surface from both the airborne ASIRAS and ESA CryoSat-2 L2i radar freeboard was closer to snow freeboard measured with ALS than it was to sea-ice freeboard measured in situ. A deep snowpack both causes negative freeboard and reduces radar penetration even at cold conditions (surface temperatures below −15°C). By treating the ESA CryoSat-2 L2i freeboard as snow freeboard and using a modified density method to convert freeboard into thickness, we obtain a sea-ice thickness distribution with mode 1.6 m, similar to that measured with HEM with mode 1.7 m. If the ESA CryoSat-2 L2i freeboard was treated as sea-ice freeboard the converted sea-ice thickness was overestimated by a factor of 2. Similar overestimated ice thickness is found, in this study region, in the NASA/AWI/CPOM data, which may result from the influence of volume scattering, from the deep snowpack we observed, on the retrieval of radar freeboard. Further studies are needed to quantify how widespread the phenomenon of limited radar penetration into snow is. If this is not considered the sea-ice thickness and mass derived from CryoSat-2, at least regionally, will have a positive bias, i.e., be too large. We urge not only an update to the snow observations as the Arctic climate regime enters a new state, but that wherever possible regional snow depth for the correct year is used to take account of interannual variability.

Acknowledgments

This work was supported by the Norwegian Polar Institute's Centre for Ice, Climate and Ecosystems (ICE) through the project N-ICE. Airborne Laser Scanner and ASIRAS data acquisitions on two flights made by the British Antarctic Survey (BAS) Twin Otter on 19 and 24 April 2015 were funded by the ICE-ARC programme from the European Union 7th Framework Program (grant 603887), ICE-ARC contribution ICE-ARC-019. This work also benefited from support from ID Arctic, a project funded by the Norwegian Ministries of Foreign Affairs and Climate and Environment, from the ESA SMOSIce project (ESA contract 4000110477/14/NL/FF/lf), and from the ESA CryoVal-SI project (4000108390/13/NL/CT). Jennifer King was funded by the Norwegian Research Council project "CORESAT" (NFR project 222681). G. Spreen was supported by the Institutional Strategy of the University of Bremen, funded by the German Excellence Initiative. We would like to thank all members of the N-ICE2015 team and the crew from R/V Lance for their help collecting and producing the N-ICE2015 data set. We thank also the crew of Airlift and the Twin Otter pilots. Special thanks are due to Marius Bratrein for assistance with HEM data collection and to Stephen Hudson, Nina Maaß, Caixin Wang, Mats Granskog, and Polona Itkin for their hard work during the field surveys on 19 and 24 April. The N-ICE2015 data are available through the Norwegian Polar Institute's Data Centre (https://data.npolar.no/home/). CryoSat-2 baseline C data are available from ESA via an ftp client (ftp://science-pds.cryosat.esa.int). The airborne campaign data (ALS and ASIRAS) are public available within the ICE-ARC project and can be found in the British Antarctic Data repository at http://ice2seadata.nerc-bas.ac.uk/repository. ERA reanalysis was obtained from http://www.ecmwf.int/en/research/climate-reanalysis/era-interim. The back tracking was performed using IFREMER data from ftp://ftp.ifremer.fr/ifremer/cersat/products/gridded/psi-drift/data/arctic/merged-quikscat-ssmi/. We would also like to thank Eero Rinne and several anonymous reviewers for their input, which has significantly improved this paper.

References

Alexandrov, V., Sandven, S., Wahlin, J., & Johannessen, O. M. (2010). The relation between sea ice thickness and freeboard in the Arctic. *The Cryosphere*, *4*, 373–380. https://doi.org/10.5194/tc-4-373-2010

Beaven, S. G., Lockhart, G. L., Gogineni, S. P., Hossetnmostafa, A. R., Jezek, K., Gow, A. J., et al. (1995). Laboratory measurements of radar backscatter from bare and snow-covered saline ice sheets. *International Journal of Remote Sensing*, *16*, 851–876. https://doi.org/10.1080/01431169508954448

Berrisford, P., Dee, D. P., Poli, P., Brugge, R., Fielding, K., Fuentes, M., et al. (2011). *The ERA-Interim archive Version 2.0* (ERA Report Series). Reading, Bershire: ECMWF.

Bintanja, R., & Selten, F. M. (2014). Future increases in Arctic precipitation linked to local evaporation and sea-ice retreat. *Nature*, *509*(7501), 479–482. https://doi.org/10.1038/nature13259

Borisch, W. (2011). *ASIRAS upgrade user manual*. Germany: RST GmbH.

Bouzinac, C. (2014). *CryoSat-2 product handbook*. London, UK: ESRIN-ESA and Mullard Space Science Laboratory, University College London. Retrieved from https://earth.esa.int/documents/10174/125272/CryoSat_Product_Handbook

Cavalieri, D. J., & Parkinson, C. L. (2012). Arctic sea ice variability and trends, 1979–2010. *The Cryosphere*, *6*, 881–889. https://doi.org/10.5194/tc-6-881-2012

Cohen, L., Hudson, S. R., Walden, V. P., & Granskog, M. A. (2017). Meteorological conditions in a thinner Arctic sea ice regime from winter through spring during the Norwegian young sea ICE expedition (N-ICE2015). *Journal of Geophysical Research: Atmospheres*, *122*, 7235–7259. https://doi.org/10.1002/2016JD026034

Comiso, J. C. (2012). Large decadal decline of the arctic multiyear ice cover. *Journal of Climate*, *25*, 1176–1193. https://doi.org/10.1175/JCLI-D-11-00113.1

Comiso, J. C., Parkinson, C. L., Gersten, R., & Stock, L. (2008). Accelerated decline in the Arctic sea ice cover. *Geophysical Research Letters*, *35*, L01703. https://doi.org/10.1029/2007GL031972

Farrell, S. L., Laxon, S. W., McAdoo, D. C., Yi, D., & Zwally, H. J. (2009). Five years of Arctic sea ice freeboard measurements from the Ice, Cloud and land Elevation Satellite. *Journal of Geophysical Research*, *114*, C04008. https://doi.org/10.1029/2008JC005074

Forsström, S., Gerland, S., & Pedersen, C. A. (2011). Thickness and density of snow-covered sea ice and hydrostatic equilibrium assumption from in situ measurements in Fram Strait, the Barents Sea and the Svalbard coast. *Annals of Glaciology*, *52*(57), 261–269.

Gallet, J.-C., Merkouriadi, I., Liston, G. E., Polashenski, C., Hudson, S. R., Rösel, A., et al. (2017). Spring snow conditions on Arctic sea ice north of Svalbard, during the Norwegian young sea ICE (N-ICE2015) expedition. *Journal of Geophysical Research: Atmospheres*, *122*, 10820–10836. https://doi.org/10.1002/2016JD026035

Gerland, S., Granskog, M. A., King, J., & Rösel, A. (2017). *N-ICE2015 ice core physics: Temperature, salinity and density* [Data set] . Norway: Norwegian Polar Institute. https://doi.org/10.21334/npolar.2017.c3db82e3

Gerland, S., Renner, A. H. H., Spreen, G., Wang, C., Beckers, J., Dumont, M., et al. (2012). In-Situ calibration and validation of CryoSat-2 observations over Arctic sea ice north of Svalbard. In *Proceedings paper (ESA-SP-712), ESA Earth Observation and Cryosphere Science Conference*, 13–16 November 2012, Frascati, Italy.

Giles, K. A., & Hvidegaard, S. M. (2006). Comparison of space borne radar altimetry and airborne laser altimetry over sea ice in the Fram Strait. *International Journal of Remote Sensing*, *27*(15), 3105–3113. https://doi.org/10.1080/01431160600563273

Giles, K. A., Laxon, S. W., Wingham, D. J., Wallis, D. W., Krabill, W. B., Leuschen, C. J., et al. (2007). Combined airborne laser and radar altimeter measurements over the Fram Strait in May 2002. *Remote Sensing of Environment*, *111*, 182–194.

Girard-Ardhuin, F., & Ezraty, R. (2012). Enhanced Arctic sea ice drift estimation merging radiometer and scatterometer data. *IEEE Transactions on Geoscience and Remote Sensing*, *50*(7), 2639–2648. https://doi.org/10.1109/TGRS.2012.2184124

Graham, R. M., Rinke, A., Cohen, L., Hudson, S. R., Walden, V. P., Granskog, M. A., et al. (2017). A comparison of the two Arctic atmospheric winter states observed during N-ICE2015 and SHEBA. *Journal of Geophysical Research: Atmosphere*, *121*, 5716–5737. https://doi.org/10.1002/2016JD025475

Granskog, M. A., Assmy, P., Gerland, S., Spreen, G., Steen, H., & Smedsrud, L. H. (2016). Arctic research on thin ice: Consequences of Arctic sea ice loss. *Eos, Transactions American Geophysical Union*, *97*(5), 22–36. https://doi.org/10.1029/2016EO044097

Granskog, M. A., Rösel, A., Dodd, P. A., Divine, D., Gerland, S., Martma, T., et al. (2017). Snow contribution to first-year and second-year Arctic sea ice mass balance north of Svalbard. *Journal of Geophysical Research: Oceans*, *122*, 2539–2549. https://doi.org/10.1002/2016JC012398.

Haas, C., Gerland, S., Eicken, H., & Miller, H. (1997). Comparison of sea-ice thickness measurements under summer and winter conditions in the Arctic using a small electromagnetic induction device. *Geophysics*, *62*, 749–757.

Haas, C., Hendricks, S., Ricker, R., King, J., Beckers, J., Skourup, H., et al. (2016). *CryoVal-SI: CryoSat Sea Ice Product Validation using CryoVex and IceBridge campaign data* (Tech. Note 3: Assessment of different sources of uncertainty). Norway: Norwegian Polar Institute.

Haas, C., Lobach, J., Hendricks, S., Rabenstein, L., & Pfaffling, A. (2009). Helicopter-borne measurements of sea ice thickness, using a small and lightweight, digital EM system. *Journal of Applied Geophysics, Airborne Geophysics*, *67*, 234–241. https://doi.org/10.1016/j.jappgeo.2008.05.005

Haas, C., Pfaffling, A., Hendricks, S., Rabenstein, L., Etienne, J.-L., & Rigor, I. (2008). Reduced ice thickness in Arctic Transpolar Drift favors rapid ice retreat. *Geophysical Research Letters*, *35*, L17501. https://doi.org/10.1029/2008GL034457

Hansen, E., Gerland, S., Granskog, M. A., Pavlova, O., Renner, A. H. H., Haapala, J., et al. (2013). Thinning of Arctic sea ice observed in Fram Strait: 1990–2011. *Journal of Geophysical Research: Oceans*, *118*, 520–5221. https://doi.org/10.1002/jgrc.20393

Helm, V., Humbert, A., & Miller, H. (2014). Elevation and elevation change of Greenland and Antarctica derived from CryoSat-2. *The Cryosphere*, *8*(4), 1539–1559. https://doi.org/10.5194/tc-8-1539-2014

Helm, V., Rack, W., Cullen, R., Nienow, P., Mair, D., Parry, V., et al. (2007). Winter accumulation in the percolation zone of Greenland measured by airborne radar altimeter. *Geophysical Research Letters*, *34*, L06501. https://doi.org/10.1029/2006GL029185

Hendricks, S., Stenseng, L., Helm, V., & Haas, C. (2010). Effects of surface roughness on sea ice freeboard retrieval with an airborne Ku-band radar and SAR radar altimeter. In *IEEE International Symposium Geoscience and Remote Sensing (IGARSS 2010)*. IEEE.

Hudson, S. R., Cohen, L., & Walden, V. P. (2015). *N-ICE2015 surface meteorology v2 [Data set]*. Norway: Norwegian Polar Institute. https://doi.org/10.21334/npolar.2015.056a61d1

Hvidegaard, S. M., & Forsberg, R. (2002). Sea-ice thickness from airborne laser altimetry over the Arctic Ocean north of Greenland. *Geophysical Research Letters*, *29*(20), 1952. https://doi.org/10.1029/2001GL014474

Itkin, P., Spreen, G., Cheng, B., Doble, M., Girard-Ardhuin, F., Haapala, J., et al. (2017). Thin ice and storms: Sea ice deformation from buoy arrays deployed during N-ICE2015. *Journal of Geophysical Research: Oceans*, *122*, 4661–4674. https://doi.org/10.1002/2016JC012403

Kern, S., Khvorostovsky, K., Skourup, H., Rinne, E., Parsakhoo, Z. S., Djepa, V., et al. (2015). The impact of snow depth, snow density and ice density on sea ice thickness retrieval from satellite radar altimetry: Results from the ESA-CCI Sea Ice ECV Project Round Robin Exercise. *The Cryosphere*, *9*, 37–52. https://doi.org/10.5194/tc-9-37-2015

Kern, S., Ozsoy-Cicek, B., & Worby, A. P. (2016). Antarctic sea-ice thickness retrieval from ICESat: Intercomparison of different approaches. *Remote Sensing*, *8*(7), 538, https://doi.org/10.3390/rs8070538

King, J., Gerland, S., Spreen, G., & Bratrein, M. (2016). *N-ICE2015 sea-ice thickness measurements from helicopter-borne electromagnetic induction sounding [Data set]*. Norway: Norwegian Polar Institute. https://doi.org/10.21334/npolar.2016.aa3a5232

Kurtz, N., & Farrell, S. L. (2011). Large-scale surveys of snow depth on Arctic sea ice from Operation IceBridge. *Geophysical Research Letters*, *38*, L20505. https://doi.org/10.1029/2011GL049216

Kurtz, N., Farrell, S. L., Studinger, M., Galin, N., Harbeck, J., Lindsay, R., et al. (2013). Sea ice thickness, freeboard, and snow depth products from Operation IceBridge airborne data. *The Cryosphere*, *7*, 1035–1056. https://doi.org/10.5194/tc-7-1035-2013

Kurtz, N., & Harbeck, J. (2017). *CryoSat-2 level-4 sea ice elevation, freeboard, and thickness, Version 1. [April 2015]*. Boulder, CO: NASA National Snow and Ice Data Center Distributed Active Archive Center. https://doi.org/10.5067/96JO0KIFDAS8

Kurtz, N. T., Galin, N., & Studinger, M. (2014). An improved CryoSat-2 sea ice freeboard retrieval algorithm through the use of waveform fitting. *The Cryosphere*, *8*, 1217–1237. https://doi.org/10.5194/tc-8-1217-2014

Kwok, R. (2014). Simulated effects of a snow layer on retrieval of CryoSat-2 sea ice freeboard. *Geophysical Research Letters*, *41*, 5014–5020. https://doi.org/10.1002/2014GL060993

Kwok, R., & Cunningham, G. F. (2008). ICESat over Arctic sea ice: Estimation of snow depth and ice thickness. *Journal of Geophysical Research*, *113*, C08010. https://doi.org/10.1029/2008JC004753

Kwok, R., & Cunningham, G. F. (2015). Variability of Arctic sea ice thickness and volume from CryoSat-2. *Philosophical Transactions of the Royal Society A*, *373*, 20140157. https://doi.org/10.1098/rsta.2014.0157

Kwok, R., & Rothrock, D. A. (2009). Decline in Arctic sea ice thickness from submarine and ICEsat records: 1958–2008. *Geophysical Research Letters*, *36*, L15501. https://doi.org/10.1029/2009GL039035

Laxon, S. W., Giles, K. A., Ridout, A. L., Wingham, D. J., Willatt, R., Cullen, R., et al. (2013). CryoSat-2 estimates of Arctic sea ice thickness and volume. *Geophysical Research Letters*, *40*, 732–737. https://doi.org/10.1002/grl.50193

Mahoney, A., Eicken, H., Fukamachi, Y., Ohshima, K. I., Simizu, D., Kambhamettu, C., et al. (2015). Taking a look at both sides of the ice: Comparison of ice thickness and drift speed as observed from moored, airborne and shore-based instruments near Barrow, Alaska. *Annals of Glaciology*, *56*(69), 363–372. https://doi.org/10.3189/2015AoG69A565

Meier, W. N., Hovelsrud, G. K., van Oort, B. E. H., Key, J. R., Kovacs, K. M., Michel, C., et al. (2014). Arctic sea ice in transformation: A review of recent observed changes and impacts on biology and human activity. *Reviews of Geophysics*, *52*, 185–217. https://doi.org/10.1002/2013RG000431

Merkouriadi, I., Gallet, J.-C., Liston, G., Polashenski, C., Itkin, P., King, J., et al. (2017). *N-ICE2015 snow pit data [Data set]*. Norway: Norwegian Polar Institute. https://doi.org/10.21334/npolar.2017.d2be5f05

Nandan, V., Geldsetzer, T., Yackel, J., Mahmud, M., Scharien, R., Howell, S., et al. (2017). Effect of snow salinity on CryoSat-2 Arctic first-year sea ice freeboard measurements. *Geophysical Research Letters*, *44*, 10419–10426. https://doi.org/10.1002/2017GL074506

Newman, T., Farrell, S. L., Richter-Menge, J., Connor, L. N., Kurtz, N. T., Elder, B. C., et al. (2014). Assessment of radar-derived snow depth over Arctic sea ice. *Journal of Geophysical Research: Oceans*, *119*, 8578–8602. https://doi.org/10.1002/2014JC010284

Park, D.-S. R., Lee, S., & Feldstein, S. B. (2015). Attribution of the recent winter sea ice decline over the Atlantic Sector of the Arctic Ocean. *Journal of Climate*, *28*(10), 4027–4033. https://doi.org/10.1175/JCLI-D-15-0042.1

Renner, A. H. H., Hendricks, S., Gerland, S., Beckers, J., Haas, C., & Krumpen, T. (2013). Large-scale ice thickness distribution of first-year sea ice in spring and summer north of Svalbard. *Annals of Glaciology*, *54*, 13–18. https://doi.org/10.3189/2013AoG62A146

Ricker, R., Hendricks, S., Helm, V., Skourup, H., & Davidson, M. (2014). Sensitivity of CryoSat-2 Arctic sea-ice freeboard and thickness on radar-waveform interpretation. *The Cryosphere*, *8*, 1607–1622. https://doi.org/10.5194/tc-8-1607-2014

Ricker, R., Hendricks, S., Perovich, D. K., Helm, V., & Gerdes, R. (2015). Impact of snow accumulation on CryoSat-2 range retrievals over Arctic sea ice: An observational approach with buoy data. *Geophysical Research Letters*, *42*, 4447–4455. https://doi.org/10.1002/2015GL064081

Rösel, A., Divine, D., King, J. A., Nicolaus, M., Spreen, G., Itkin, P., et al. (2016). *N-ICE2015 total (snow and ice) thickness data from EM31*[Data set] . Norway: Norwegian Polar Institute. https://doi.org/10.21334/npolar.2016.70352512

Rösel, A., King, J., Doulgeris, A., Wagner, P., Johansson, A., & Gerland, S. (2017). Can we extend local sea-ice measurements to satellite scale? An example from the N-ICE2015 expedition. *Annals of Glaciology*, 1–10. https://doi.org/10.1017/aog.2017.37

Rösel, A., Itkin, P., King, J., Divine, D., Wang, C., Granskog, M. A., et al. (2018). Thin sea ice, thick snow and widespread negative freeboard observed during N-ICE2015 north of Svalbard. *Journal of Geophysical Research: Oceans.* https://doi.org/10.1002/2017JC012865

Rösel, A., & King, J. (2017). *N-ICE2015 ice thickness, snow thickness, and freeboard from thickness drillings*[Data set] . Norway: Norwegian Polar Institute. https://doi.org/10.21334/npolar.2017.25f70db1

Rösel, A., Polashenski, C. M., Liston, G. E., King, J. A., Nicolaus, M., Gallet, J.-C., et al. (2016). N-*ICE2015 snow depth data with Magna Probe*[– Data set] . Norway: Norwegian Polar Institute. https://doi.org/10.21334/npolar.2016.3d72756d

Spreen, G., Kwok, R., Menemenlis, D., & Nguyen, A. T. (2016). Sea-ice deformation in a coupled ocean-sea-ice model and in satellite remote sensing data. *The Cryosphere Discuss*, *11*, 1553–1573. https://doi.org/10.5194/tc-2016-13

Tilling, R. L., Ridout, A., & Shepherd, A. (2016). Near-real-time Arctic sea ice thickness and volume from CryoSat-2. *The Cryosphere*, *10*, 2003–2012. https://doi.org/10.5194/tc-10-2003-2016

Tilling, R. L., Ridout, A., Shepherd, A., & Wingham, D. J. (2015). Increased Arctic sea ice volume after anomalously low melting in 2013. *Nature Geoscience*, *8*, 643–646. https://doi.org/10.1038/ngeo2489

Warren, S. G., Rigor, I. G., Untersteiner, N., Radionov, V. F., Bryazgin, N. N., Aleksandrov, Y. I., et al. (1999). Snow depth on Arctic sea ice. *Journal of Climate*, *12*, 1814–1829. https://doi.org/10.1175/1520-0442(1999)012<1814:SDOASI>2.0.CO;2

Webster, M. A., Rigor, I. G., Nghiem, S. V., Kurtz, N. T., Farrell, S. L., Perovich, D. K., et al. (2014). Interdecadal changes in snow depth on Arctic sea ice. *Journal of Geophysical Research: Oceans*, *119*, 5395–5406. https://doi.org/10.1002/2014JC009985

Wingham, D. J., Francis, C. R., Baker, S., Bouzinac, C., Brockley, D., Cullen, R., et al. (2006). CryoSat: A mission to determine the fluctuations in Earth's land and marine ice fields. *Advances in Space Research*, *37*, 841–871. https://doi.org/10.1016/j.asr.2005.07.027

Wingham, D. J., Phalippou, L., Mavrocordatos, C., & Wallis, D. (2004). The mean echo and echo cross product from a beamforming interferometric altimeter and their application to elevation measurement. *IEEE Transactions on Geoscience and Remote Sensing*, *42*(10), 2305–2323. https://doi.org/10.1109/TGRS.2004.834352

Willatt, R., Laxon, S., Giles, K., Cullen, R., Haas, C., & Helm, V. (2011). Ku-band radar penetration into snow cover on Arctic sea ice using airborne data. *Annals of Glaciology*, *52*, 197–205.

Willatt, R. C., Giles, K., Laxon, S. W., Stone-Drake, L., & Worby, A. (2010). Field investigations of Ku-band radar penetration into snow cover on Antarctic Sea Ice. *IEEE Transactions on Geoscience and Remote Sensing*, *48*, 365–372. https://doi.org/10.1109/TGRS.2009.2028237

Woods, C., & Caballero, R. (2016). The role of moist intrusions in winter arctic warming and sea ice decline. *Journal of Climate*, *29*(12), 4473–4485. https://doi.org/10.1175/jcli-d-15-0773.1

Zwally, H. J., Schutz, B., Abdalati, W., Abshire, J., Bentley, C., Brenner, A., et al. (2002). ICESat's laser measurements of polar ice, atmosphere, ocean, and land. *Journal of Geodynamics*, *34*(3–4), 405–445. https://doi.org/10.1016/S0264-3707(02)00042-X